SCIENTIFIC REPORTS

OPEN

SUBJECT AREAS:
ELECTRONIC STRUCTURE
PHOTOCATALYSIS

Received
30 June 2014

Accepted
1 December 2014

Published
19 January 2015

Correspondence and requests for materials should be addressed to F.T. (tfwd@163.com)

An Innovative Anion Regulation Strategy for Energy Bands of Semiconductors: A Case from Bi_2O_3 to $Bi_2O(OH)_2SO_4$

Hao Tian[1,2], Fei Teng[1,2,3,4], Juan Xu[1,2], Sunqi Lou[1,2], Na Li[1,2], Yunxuan Zhao[1,2] & Mindong Chen[1,2,3,4]

[1]Jiangsu Engineering and Technology Research Center of Environmental Cleaning Materials (ECM), School of Environmental Science and Engineering, Nanjing University of Information Science & Technology, 219 Ningliu Road, Nanjing 210044, China, [2]Jiangsu Key Laboratory of Atmospheric Environment Monitoring and Pollution Control (AEMPC), School of Environmental Science and Engineering, Nanjing University of Information Science & Technology, 219 Ningliu Road, Nanjing 210044, China, [3]Jiangsu Joint Laboratory of Atmospheric Pollution Control (APC), School of Environmental Science and Engineering, Nanjing University of Information Science & Technology, 219 Ningliu Road, Nanjing 210044, China, [4]Collaborative Innovation Center of Atmospheric Environment and Equipment Technology (AEET), School of Environmental Science and Engineering, Nanjing University of Information Science & Technology, 219 Ningliu Road, Nanjing 210044, China.

How to develop a new, efficient photo catalyst is still a big challenge to us. A suitable band gap is the key for light absorption of semiconductor. Herein, an innovative anion intercalation strategy is, for the first time, developed to regulate the energy band of semiconductor. Typically, we introduce a layered sulfate compound ($Bi_2O(OH)_2SO_4$) as a new photo catalyst, which has not been known before. Both partial density of states (PDOS) and total density of states (TDOS) have demonstrated that compared with Bi_2O_3 (2.85 eV), the band gap of $Bi_2O(OH)_2SO_4$ has been widened to 4.18 eV by the intercalation of sulfate anion. Moreover, the band gap width of oxyacid salt compound is mainly predominated by the number of the outmost electrons (NOE) of central atom of anion. This study suggests that new photo catalysts can be developed by grouping anions with the existing oxides or sulfides.

Since the first report by Fujishima and Honda[1], photo catalysis has been researched extensively[2,3], which only utilizes abundant solar energy[4]. Up to now, a variety of semiconductors photo catalysts have been developed including oxides[5], sulfides[6], oxysalts[7] and polymers[8] and many efforts have been made to explore beneficial structure[9] and suitable compositions[10,11]. Regrettably, the practical applications are limited by the low quantum efficiency, light utilization efficiency and photo activity. Thus, it is still a big challenge to develop the efficient, inexpensive photo catalysts, which would greatly promote the applications of this technology in practices.

Recently, nonmetal oxyacid salts have attracted significant attentions from researchers.[12–18] Ye *et al.*[12] have reported that Ag_3PO_4 has an outstanding photo oxidation activity, and they have further suggested that the new oxyacid salts photo catalysts could be potentially developed through combining *p*-block nonmetal elements (*e.g.*, B, P, S, *etc.*) with binary oxide (*e.g.*, Bi_2O_3, Cu_2O, *etc.*). This prediction can be demonstrated by an efficient $BiPO_4$ photo catalyst[13]. Zhu *et al.*[13] have revealed that it is the inductive effect of large dipole resultant from negatively-charged PO_4^{3-} anion that benefits the photogenerated charge separation. Besides $BiPO_4$ and Ag_3PO_4[13–15], the other oxyacid salts containing nonmetals have also been reported to have higher activities than titania, including Bi_3O_4Cl[16], $Bi_2O_2CO_3$[17] and $Cu_2(OH)PO_4$[18], and so on. In these cases, the characteristic layered structure of $(Bi_2O_2)^{2+}$ is believed to produce an internal electric field that is favorable for the efficient separation and transfer of photogenerated electrons and holes. Furthermore, Bi-based semiconductors are also found to possess the hybridized energy band structures on account of the lone pair electrons of bismuth, which can effectively inhibit the recombination of photogenerated electrons and holes[12–15]. Besides, the hydroxyl-containing photo catalysts with wide band gaps have also been found to have the strong photo oxidation abilities for organic pollutants[19–21]. First, the highly-positive valence band has not only endowed the photogenerated holes with a strong oxidizing ability, leading to the complete mineralization of organic pollutants without forming intermediate chemicals; Second, the abundant OH groups on crystal surfaces facilitate the formation of the reactive hydroxyl radicals ($E^o(\cdot OH/OH^-) = 2.38$ eV). The complete mineralization is beneficial to maintain a clean surface and stable activity of photo catalyst. Furthermore, it has been reported[22] that sulfate anion-modification of TiO_2 can increase the decolonization rate due to the intrinsic attribution of sulfate anion: i) its strong bonding ability with H_2O

favors for the formation of ·OH; ii) its high negative charge favors to draw holes to the interface by electrostatic force[10], leading to an efficient separation of photogenerated charges. Meanwhile, the layered $Bi_2O_2[BO_2(OH)]$ has been developed as an efficient photo catalyst and its photo activity is 2.5 times higher than commercial rutile TiO_2 for the degradation of methylene blue (MB)[23]. On base of the reports above, we could expect that the $Bi_2O(OH)_2SO_4$ compound, simultaneously containing Bi, OH and SO_4^{2-}, may be a new, inexpensive, promising photo catalyst. Among nonmetal oxyacid semiconductors, nevertheless, the $Bi_2O(OH)_2SO_4$ compound as a photo catalyst has not been reported to date.

Herein, we introduce the hydroxyl-containing layered sulfate compound ($Bi_2O(OH)_2SO_4$) as a new photo catalyst. First, the $Bi_2O(OH)_2SO_4$ compound is prepared by a simple water-bath method. Secondly, theory simulation method is employed to analyze its crystal, electronic and energy band structures. Finally, we have mainly revealed the essential correlation of its activity with energy band and crystal structures. The innovative contribution of the study includes: i) The layered sulfate compound ($Bi_2O(OH)_2SO_4$) is found to have a high photo catalytic activity, which has been unknown before; ii) Compared with Bi_2O_3, the intercalation of sulfate anions have adjusted the energy band structure of $Bi_2O(OH)_2SO_4$; and as a general strategy, it can also suitable for $Bi_2O_2[BO_2(OH)]$, $Bi_2O_2CO_3$, $Bi_2O_2[NO_3(OH)]$, *etc.* iii) The regulation strategy of energy band provides us a novel idea to find new photo catalysts, namely, various new photo catalysts can be developed by grouping anions with the existing oxides or sulfides photo catalysts.

Results

Crystal structures of $Bi_2O(OH)_2SO_4$. Figure 1(a) presents the crystal structure model of $Bi_2O(OH)_2SO_4$. It has a monoclinic space group (*P21/c*) with the unit cell parameters of a = 7.692(3)Å, b = 13.87(1)Å, c = 5.688(2)Å and β = 109.01(3)° [24]. It consists of sulfate anions groups and $[Bi_2O(OH)_2^{2+}]_n$ double chains, with a featured layered structure. According to crystallographic data, the polycations double chains (Figure 1(b)) are constructed by four-member ring (Bi(1)-OH(1)-Bi(2)-O) and six-member ring (Bi(1)-OH(2)-Bi(2)-O-Bi(1)-O). It is observed that each hydroxyl (OH) group connects two Bi atoms, and each O atom connects three Bi atoms. The coordination spheres of both Bi(1) and Bi(2) are completed by the redundant O atoms of SO_4^{2-} anion. It is noteworthy that the distance of between OH(1) and O(4) is calculated to be 2.77(1) Å (Figure 1(c)), indicating that a hydrogen bond can form between them, which favors to stabilize the whole structure. These hydroxyl groups are verified by infrared spectra (IR) (Figure S1, seeing electronic supporting information (ESI)). In particular, the $[Bi_2O(OH)_2^{2+}]_n$ polycations double chains can only extend along the [001] direction, as known from the net structure of $[Bi_2O_2]^{2+}$ in Aurivillius-phase (*e.g.*, Bi_2MoO_6[25], Bi_2WO_6[26], Bi_2SiO_5[27]) or Sillen-phase (*e.g.*, BiOX, X = Cl, Br, and I)[28]. This interesting

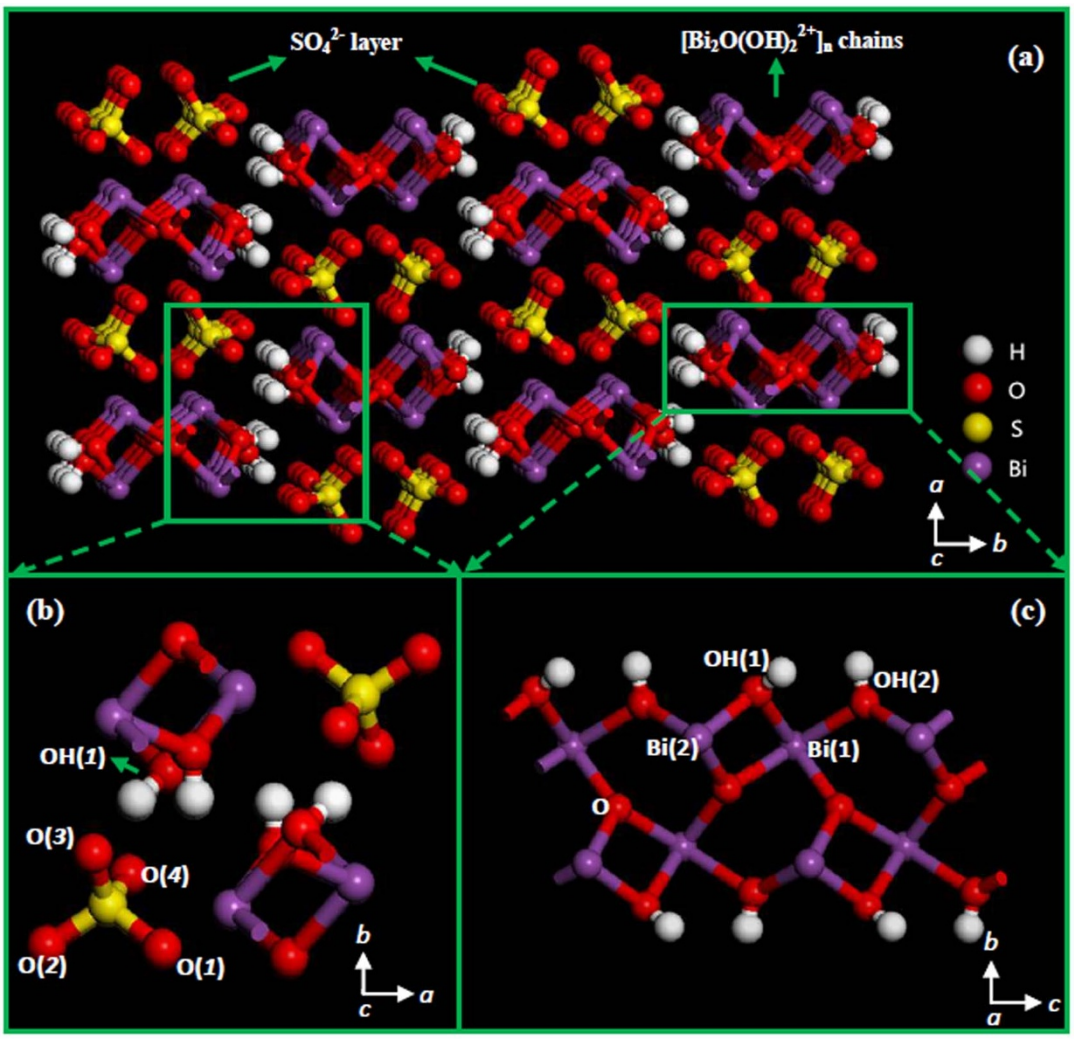

Figure 1 | (a) Crystal structure of $Bi_2O(OH)_2SO_4$; (b) The projection figure of $[Bi_2O(OH)_2^{2+}]_n$ polycations along *a* axis; (c) Environment of OH(1)-O(4) hydrogen bond.

characteristic results from the involvement of negative hydroxyl groups.

The $Bi_2O(OH)_2SO_4$ sample was prepared by a water-bath method. Figure S2 (Seeing ESI) shows the X-ray diffraction (XRD) patterns of the-prepared sample. All the diffraction peaks are well in agreement with the standard card (JCPDS 761102). No impurities peaks, e.g., $Bi(OH)_3$ or Bi_2O_3 or Bi, are observed, which confirms the formation of phase-pure $Bi_2O(OH)_2SO_4$. Figure S3 (Seeing ESI) presents the scanning electron microscopy (SEM) and transmission electron microscopy (TEM) of the as-prepared sample. It is obvious that the $Bi_2O(OH)_2SO_4$ flowers form, which are self-assembled by the nanorods of (1–1.5) μm × 0.5 μm. Its single crystalline nature has been revealed by the electron diffraction pattern (ED). Furthermore, $Bi_2O(OH)_2SO_4$ has a small solubility product value of 1.8×10^{-31} [29], meaning a good stability in an aqueous media. The pH value of supernatant is 1–2 after preparation, indicating that $Bi_2O(OH)_2SO_4$ is also stable under acidic condition.

Optical property and band gap of $Bi_2O(OH)_2SO_4$. Figure 2 and Figure S4 (Seeing ESI) show the ultraviolet-visible diffusion reflectance spectra (UV-DRS) of $Bi_2O(OH)_2SO_4$. In the absorption edge region of semiconductor, the square of absorption coefficient is linear with direct optical transition energy, whereas the square root of absorption coefficient linear with indirect optical transition energy[30]. As observed from the inset of Figure 2, the plots of absorbency^2 ($(\alpha h\nu)^2$) and absorbency$^{1/2}$ ($(\alpha h\nu)^{1/2}$) *vs.* photon energy ($h\nu$) in the absorption edge region are different: the plot of $(\alpha h\nu)^2$ *vs.* $h\nu$ is nearly linear, while the plot of $(\alpha h\nu)^{1/2}$ *vs.* $h\nu$ deviates from the fitted straight line. Hence, we could hold that the absorption edge of $Bi_2O(OH)_2SO_4$ is caused by direct optical transition. The optical band gap of $Bi_2O(OH)_2SO_4$ can be determined by Equation (1) as follows.

$$ah\nu = A(h\nu - E_g)^{n/2} \quad (1)$$

where n is dependent on the optical transition type of a semiconductor (n = 1, direct absorption; n = 4, indirect absorption)[31], α, ν, A and E_g represent absorption coefficient, photon frequency, proportionality constant and band gap, respectively. From the plot of $(\alpha h\nu)^2$ *vs.* $h\nu$, the direct band gap of $Bi_2O(OH)_2SO_4$ is determined to be 4.18 *eV*, corresponding to an optical absorption edge of 302 nm (Figure S4). It is obvious that $Bi_2O(OH)_2SO_4$ has a wider band gap than Bi_2O_3 (Figure 3). Moreover, we have calculated the positions of conduction band (E_{CB}) and valence bands (E_{VB}) using Equations (2) and (3) as follows, respectively[32].

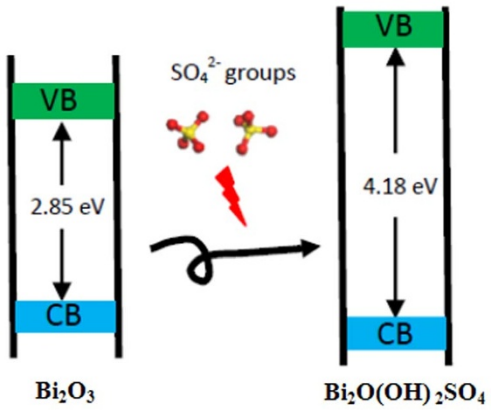

Figure 3 | The energy bands position of Bi_2O_3 and $Bi_2O(OH)_2SO_4$.

$$E_{CB} = \chi - E_e - 0.5E_g \quad (2)$$

$$E_{VB} = \chi - E_e + 0.5E_g \quad (3)$$

Where χ is the geometric mean of Mulliken's electronegativities of constituent atoms, E_e is the energy of free electrons at the hydrogen scale (~4.5 *eV*), and E_g is the band gap. The χ value is calculated to be 6.80 *eV*, E_{VB} and E_{CB} are determined to be 4.39 and 0.21 *eV*, respectively. The highly positive valence band suggests that $Bi_2O(OH)_2SO_4$ may have a high oxidation ability, which favors for the complete oxidation of organic dye.

Effect of sulfate anion and electronic structure. The *Ab* initio density functional theory (DFT) calculations have been carried out to insight the electronic structures of $Bi_2O(OH)_2SO_4$. Figure 4(a) shows its band structure calculated by the CASTEP package. Both valence band maximum (VBM) and conduction band minimum

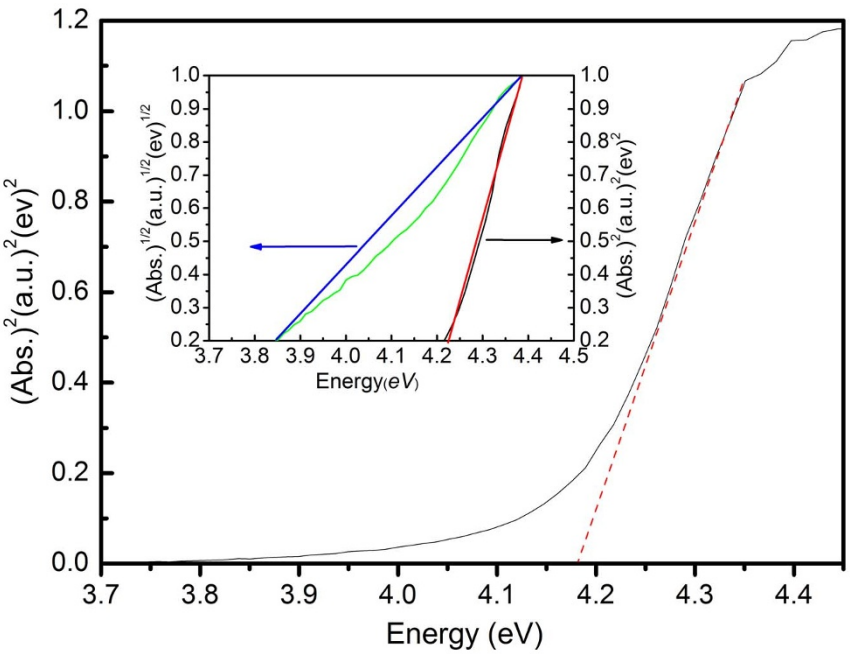

Figure 2 | Tauc plots ($(\alpha h\nu)^2$ *vs.* $h\nu$)) of $Bi_2O(OH)_2SO_4$ (the inset of both $(\alpha h\nu)^{1/2}$ and $(\alpha h\nu)^2$ *vs.* $h\nu$ in the absorption edge region).

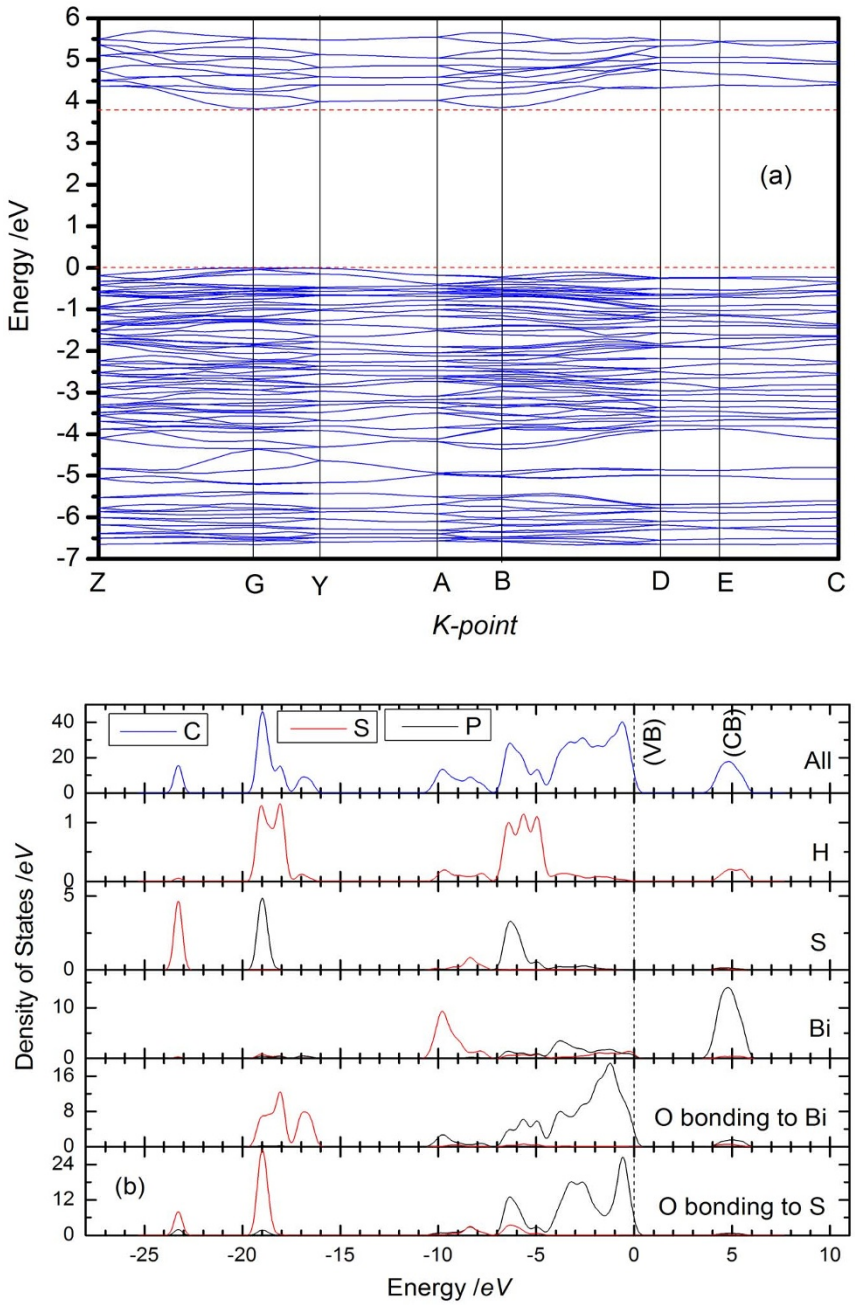

Figure 4 | (a) Electronic state structures of energy band and (b) Total and partial density of state (TDOS and PDOS) of $Bi_2O(OH)_2SO_4$: The vertical dash line represents the valence band maximum (VBM).

(CBM) at the G point further confirm the direct band gap property of $Bi_2O(OH)_2SO_4$, in good agreement with the feature of the measured absorption spectrum. Meanwhile, the indirect transition from G point to B point is also allowed, in that the indirect band gap and the direct band gap at G point are fairly close energetically. The direct band gap between VBM and CBM is 3.88 eV, with an expected diminution that is frequently pointed out as a common feature of DFT calculations[33]. For Bi-based semiconductors, it is always found that the Bi 6s and O 2p orbits could form a preferable hybridized valence band (VB)[34]. Accordingly, a reasonable dispersed energy can be observed in Figure 4(a), which would favor the transportation of the photogenerated electrons and holes, thus improving the photo catalytic activity[35].

The total density of states (DOS) and the partial DOS (Figure 4(b)) are employed to explore the electronic properties of $Bi_2O(OH)_2SO_4$. Several characteristics can be concluded as follows: (i) the VB upper of $Bi_2O(OH)_2SO_4$ is found to be not only composed of O 2p orbital, but also a little of Bi 6s and 6p orbits; while the CB bottom is dominantly composed of the Bi 6p orbital, rather than O 2p orbital. This characteristics are similar to $CaBiO_2Cl$[36], $Bi_2O_2[BO_2(OH)]$[23], and so on; (ii) In SO_4^{2-} group, a significant hybridization can be observed among S 3s, 3p and O 2p orbits located at −23 eV and −19 eV, respectively. The hybridization in VB favors for the formation of stable chemical bonds between oxygen and sulfur; (iii) At the energies higher than −5 eV, the H 1s and S 3s, 3p orbits contribute little to the VB top or CB bottom; (iv) The contribution of electronic state distribution of O (bonding to S) orbit to VB top seems much larger than that of O (bonding to Bi) orbit; (v) A large orbit hybridization occurs between H 1s orbits and O (bonding to Bi and S) orbits; (vi) For $Bi_2O(OH)_2SO_4$, the charge transfer upon photo exciting occurs from the hybrid orbits of both O 2p and Bi 6s to the empty Bi 6p orbit. It is noted that the electronic structure can provide an important

Table 1 | Band gap (E_g), VBM (E_{VB}), CBM (E_{CB}) and NOE of four compounds

Chemicals	*χ(eV)	E_g(eV)	E_{VB}(eV)	*E_{CB}(eV)	NOE
$Bi_2O_2[(OH)BO_2]$	6.34	2.85[23]	3.26	0.41	3
$Bi_2O_2CO_3$	6.54	3.10[17]	3.59	0.49	4
$Bi_2O_2[(OH)NO_3]$	6.80	3.54[48]	4.07	0.53	5
$Bi_2O(OH)_2SO_4$	6.80	4.18	4.39	0.21	6

*Notes: χ, Geometric mean of Mulliken's electronegativities; E_g, Band gap; VBM, Valence band maximum; CBM, Conduction band minimum; NOE, Number of outmost electron.

insight into the physicochemical behavior of materials. In fact, O (in SO_4^{2-}) 2p orbit predominantly constitutes the VB top, but the contribution of H to band edge is negligible, suggesting that the addition of sulfate anion can adjust the band structure, thus resulting in a higher positive VB of $Bi_2O(OH)_2SO_4$ than that of Bi_2O_3 (E_{VB} = 2.85 eV)[37]. Moreover, a large hybridization between H 1s and O2p (in SO_4^{2-}) orbits has evidenced the existence of hydrogen bonds (OH(*1*) to O(*4*)), which benefits to stabilize the $Bi_2O(OH)_2SO_4$ structure.

To further understand the role of SO_4^{2-} anion in the energy band structure of $Bi_2O(OH)_2SO_4$, we have compared four typical Bi-based oxyacid compounds with the similar layered structure. Table 1 list the E_{VB} and E_{CB} values of four Bi-based oxyacid compounds, which are calculated by Eq. (3) and (4) above. Among the four compounds, all the central atoms (B, C, N and S) in the anions locate in p block, and their numbers of the outmost electrons (NOE) increase in order. Their CBM values are positive, meaning that they cannot be used to directly acquire H_2 by water splitting. It is obviously observed from Figure 5 that both band gap and VBM value are positively correlated to the NOE of central atom. In other words, the type of anion appears to be a crucial factor to evaluate the intrinsic band structure and redox power of the semiconductors, but not an accidental. Walsh *et al.*[38] hold that the new ternary compounds photo catalysts (*e.g.*, $Bi_{20}TiO_{32}$, $SnNb_2O_6$, and $BiVO_4$, *etc.*) can be produced by combining nd^0 cations (*e.g.*, Ti^{4+}, V^{5+}, Nb^{5+}) and ns^2 cations (*e.g.*, Bi^{3+}, Sn^{2+}), and that this combination would have a significant influence on the ground-state electronic structure and the associated optical absorption. Although the essential causality of this phenomenon is still unclear, we are convinced that the wide band gap of $Bi_2O(OH)_2SO_4$ originates from the involvement of sulfate anions, as confirmed by the PDOS results. Herein, two main assumptions can be made as follows: (i) For aluminates (MAl_2O_4, M = Mg, Zn, Cu) and borates (*e.g.*, $Cu(BO_2)_2$, $Ni(BO_2)_2$), a similar band gaps could be expected in consideration of the same NOEs of anions as that of $Bi_2O_2[BO_2(OH)]$. As a result, these compounds are expected to be the promising photo catalysts driven under visible light, for example, $BiVO_4$[39],Bi_2MoO_6[40] and $SrNbO_3$[2], with the NOEs of anionic central atoms no more than 2, have exhibited excellent photo catalytic properties under visible light irradiation; MAl_2O_4 (M = Mg, Zn, Cu)[41] are also reported to have high photo catalytic activity for the degradations of dyes under visible light irradiation. (ii) The selenites (*e.g.*, $CuSeO_3$, $ZnSeO_3$) and the other sulfate semiconductors (*e.g.*, $Bi_2O(OH)_2SO_4$) could be the excellent photo catalysts due to their same NOEs. Our viewpoints as mentioned above can be demonstrated by the other reports[2,39–41]

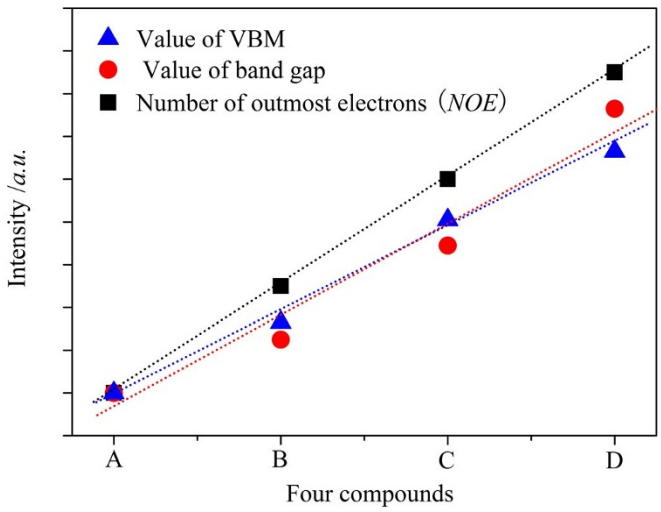

Figure 5 | Variation of band gap, VBM value, and the number of outmost electrons (NOE) of central atoms in anions of four compounds: (A) $Bi_2O_2[BO_2(OH)]$; (B) $Bi_2O_2CO_3$; (C) $Bi_2O_2[NO_3(OH)]$; (D) $Bi_2O(OH)_2SO_4$.

Photo catalytic properties. Rhodmine B (RhB) is chosen as a probe molecule to evaluate the photo catalytic performances of the samples. Figure 6(a) shows the degradation curves of RhB over the $Bi_2O(OH)_2SO_4$ and commercial rutile TiO_2. After 50 min, 71% of RhB can be degraded by $Bi_2O(OH)_2SO_4$, while only 31% of RhB is degraded by commercial rutile TiO_2, demonstrating a high photo oxidizing ability of $Bi_2O(OH)_2SO_4$. In Figure 6, the apparent reaction rate constants (k_a) are determined to be 0.024 min^{-1} and 0.0076 min^{-1} for $Bi_2O(OH)_2SO_4$ and commercial rutile TiO_2, respectively; and the degradation rate of RhB over $Bi_2O(OH)_2SO_4$ is 2.16 times faster than that of the latter. To increase light response spectra of $Bi_2O(OH)_2SO_4$, a $Bi_2O(OH)_2SO_4/Bi_2O_3$ composite has been synthesized via a facile hydrothermal method. The XRD and SEM results (Figures S5 and S6 of ESI) confirm the formation of $Bi_2O(OH)_2SO_4/Bi_2O_3$. However, $Bi_2O(OH)_2SO_4/Bi_2O_3$ composite does not show an improved photoelectrical performances, compared with Bi_2O_3 (Figures S7–S9 of ESI), because their energy band are mismatched and the $Bi_2O(OH)_2SO_4$ supported on the Bi_2O_3 surface has reduced the light absorption of Bi_2O_3. The extensive work will be carried out to further improve its performance in future.

In Figure 6(c), the trapping experiments for holes and radicals have been performed to explore the photo catalytic degradation process, in which ammonium oxalate and dimethylsulfoxide (DMSO) are used as the hole scavenger[42] and the radical scavenger[43], respectively. The photo catalytic activity of $Bi_2O(OH)_2SO_4$ decreases slightly when adding 1 mmol ammonium oxalate, while the degradation reaction is obviously inhibited when adding 10 mL DMSO. This indicates that the hydroxyl radicals are the major active oxidative species for RhB over the $Bi_2O(OH)_2SO_4$ photo catalyst. To understand its stability, we have further investigated the XRD patterns of the sample after photo catalytic reaction (Figure S2 of ESI). It is obvious that its crystallinity decreases fairly slightly, indicating a high stability of $Bi_2O(OH)_2SO_4$. Thus, $Bi_2O(OH)_2SO_4$ could be a promising, efficient photo catalyst in consideration of its low cost, high stability and strong photo oxidation ability.

Photo electrochemical properties. Electrochemical impedance spectroscopy (EIS) is measured to investigate the electron transfer (Figure 7). Under UV illumination, the semicircle radius of $Bi_2O(OH)_2SO_4$ electrode is obviously smaller than that under darkness. Also, its semicircle radius is significantly smaller than

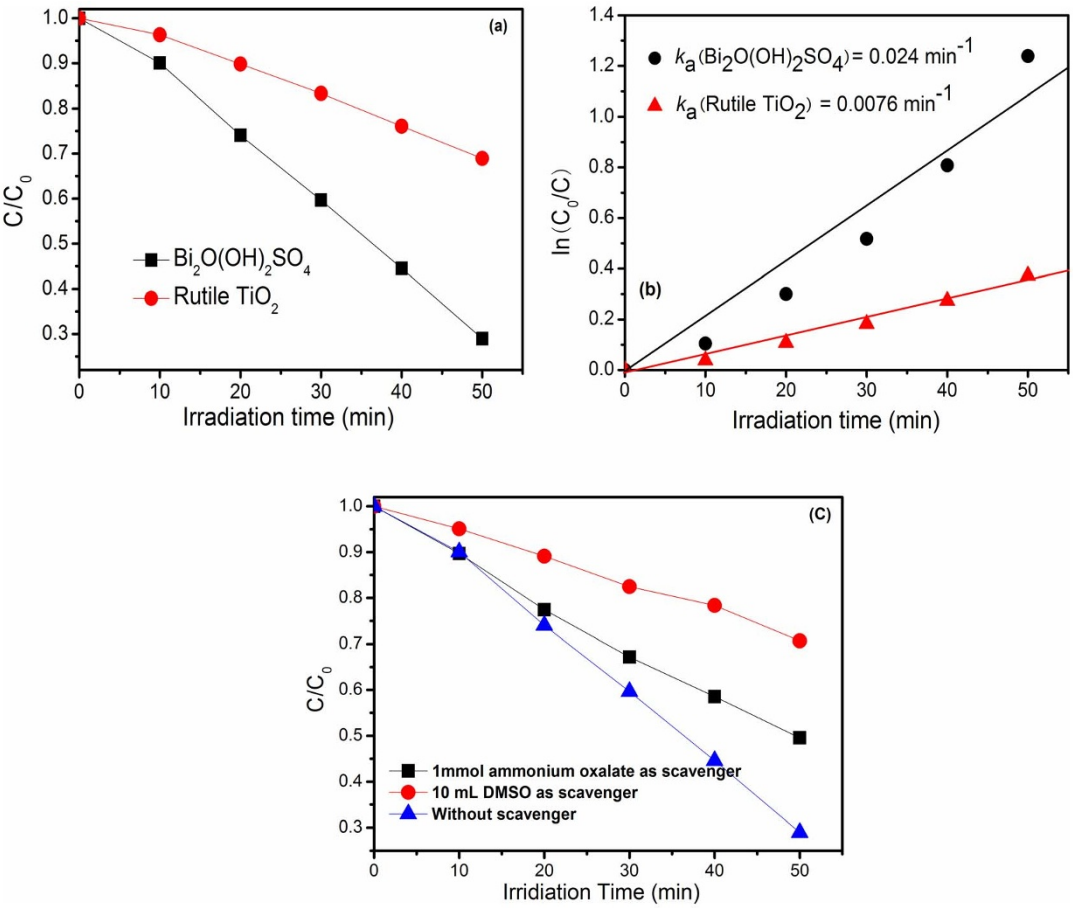

Figure 6 | Degradation curves (a) and reaction kinetic curves (b) of RhB over $Bi_2O(OH)_2SO_4$ and commercial rutile TiO_2; (c) effect of scavenger on the degradation activity of RhB over $Bi_2O(OH)_2SO_4$ under ultraviolet light irradiation ($\lambda < 420$ nm).

that of commercial rutile TiO_2 under UV illumination or darkness. A smaller semicircle radius in Nyquist plot means a smaller electric resistance of electrode, which favor for electron transfer, thus leading to an efficient charge separation[44]. Therefore, we hold that the intrinsic layer structure of $Bi_2O(OH)_2SO_4$ favors for the transfer and separation of electron-hole pairs, leading to an improved photo catalytic properties.

The photo catalytic activity of material can be directly reflected by the transient photocurrent generated under light illumination[45]. As shown in Figure 8, the photocurrent of $Bi_2O(OH)_2SO_4$ electrode can continuously generate while light-on, and its photocurrent density is greatly larger than that of commercial rutile TiO_2. The unique layer structure may favor for the separation and transfer of charges. The result is in accord with the order of photo catalytic activity, because

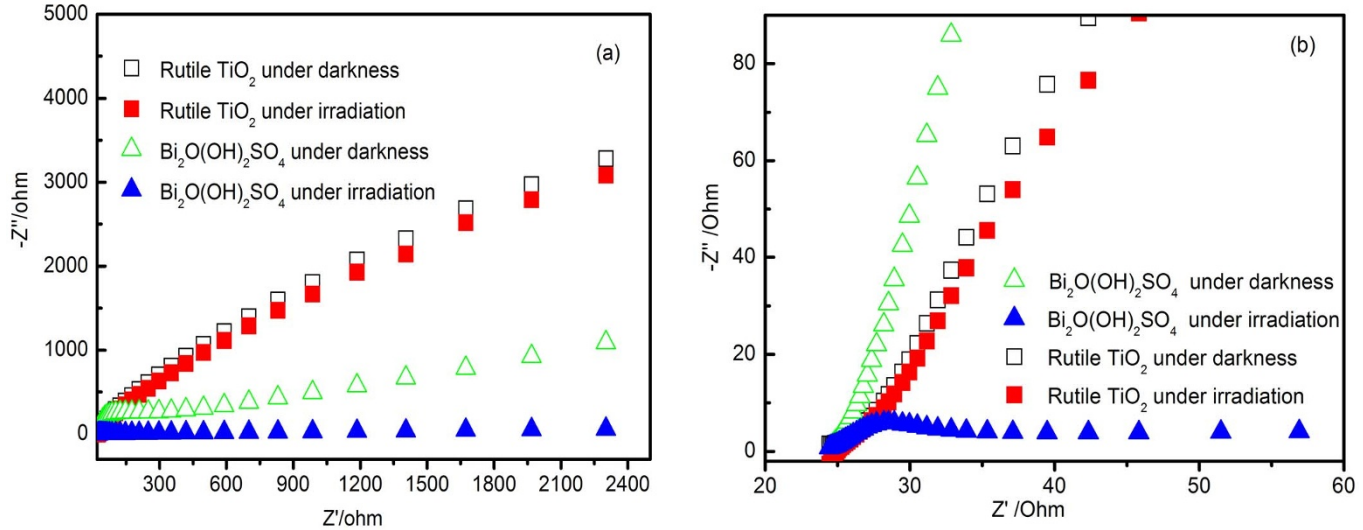

Figure 7 | Nyquist plots of $Bi_2O(OH)_2SO_4$ and commercial rutile TiO_2 under UV light-on and -off ($\lambda < 420$ nm) in 1 M KNO_3 aqueous solution: (a) in the whole frequency range; (b) in the high frequency range.

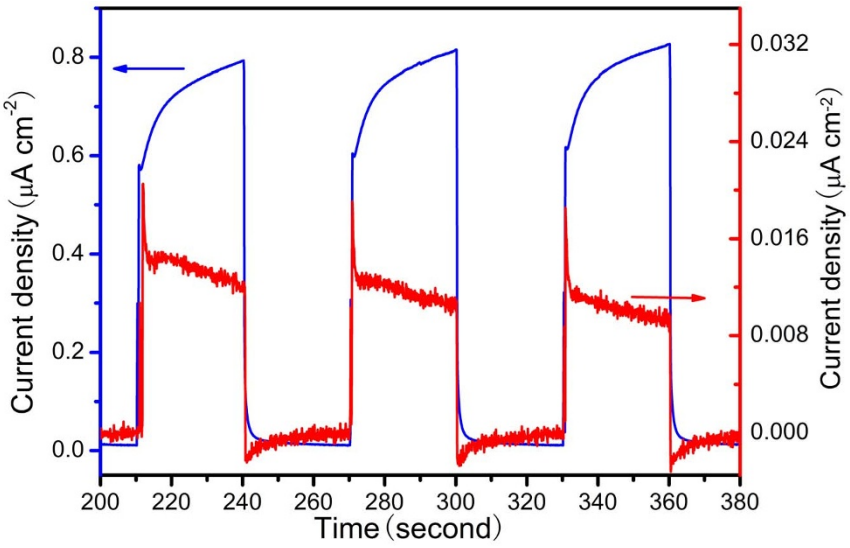

Figure 8 | Transient photocurrent responses of $Bi_2O(OH)_2SO_4$ (Blue curve) and commercial rutile TiO_2 (Red curve) under UV light irradiation (λ = 254 nm) in 0.1 M Na_2SO_4 aqueous solution.

the generation of photogenerated carriers is a critical step of photo catalytic reactions. The result demonstrates an excellent photo catalytic performances of $Bi_2O(OH)_2SO_4$. Besides, an incident photon-to-electron conversion efficiency (IPCE) measurement was performed. However, a very small efficiency or almost no photon-to-electron conversion can be observed in wavelength range of 200–800 nm in our experiment (Figure S11 of ESI). It is because the light intensity is fairly weak at light wavelengths shorter than 300 nm for the Xe lamp.

Discussion

The BET area of $Bi_2O(OH)_2SO_4$ is determined to be 9.8 $m^2\ g^{-1}$, which is only one fifth of that (50 m^2g^{-1}) of commercial rutile TiO_2. Its high degradation activity seems closely relative to the characteristic layer structure that may favor for the separation and transfer of charges. Herein, we hold that two main factors play an important role in the photo catalytic oxidation of RhB dye: (i) the separation and transfer efficiencies of photogenerated electrons and holes; (ii) the number of the formed ·OH radicals.

First, the $[Bi_2O(OH)_2^{2+}]_n$ double chains extend along the [001] direction, and they independently interleave with the slab of SO_4^{2-} to form an unique layered structure. The layered structure would lead to an internal electric field perpendicular to the cationic $[Bi_2O(OH)_2^{2+}]_n$ slab and anionic SO_4^{2-} slab, similar to BiOCl[46]. This internal electric field, different somewhat from BiOCl, is also parallel to anionic SO_4^{2-} slab, which result from the intervened arrangement of $[Bi_2O(OH)_2^{2+}]_n$ double chains. Strikingly, a strong electrostatic force can be produced by the large negatively charged SO_4^{2-} anions than Cl^- anions. Therefore, its unique layered structure may be mainly responsible for the efficient separation of photogenerated electrons and holes. Summarily, the photo catalytic activity of $Bi_2O(OH)_2SO_4$ can be significantly improved by the efficient separation and transfer of chares, as confirmed by the EIS and photocurrent results above.

Second, $Bi_2O(OH)_2SO_4$ has a more positive E_{VB} (4.39 eV) due to the intercalation of anionic sulfate, compared with Bi_2O_3 (2.85 eV), TiO_2 (2.7 eV) and E^o (·OH/OH^-) = 2.38 eV. As a result, the highly positive holes generated over $Bi_2O(OH)_2SO_4$ are thermodynamically favorable to react with H_2O and/or OH^- to produce more ·OH radicals. Thus, the ·OH radicals and/or highly positive holes result in the mineralization of organic dyes. Meanwhile, the intercalated SO_4^{2-}, with a highly negative electrostatic force, has a strong bonding ability with H_2O molecules, and also favors to draw the holes to the surface. As a result, the photo catalytic performance of $Bi_2O(OH)_2SO_4$. can be improved effectively.

Third, we hold that a synergetic effect between OH^- and SO_4^{2-} play an important role in the improved performance of $Bi_2O(OH)_2SO_4$. The OH^- anions are necessary to capture the photogenerated holes to form hydroxyl radicals, while the negatively charged SO_4^{2-} groups would prefer to attract the positive holes and repel the negative electrons. The other researchers[19,20,47] have also reported that under light excitation, the OH^- anions in crystal structure are easy to form hydroxyl radicals. Therefore, more reactive ·OH can be produced over $Bi_2O(OH)_2SO_4$ due to the co-presence of both OH^- and SO_4^{2-}, leading to a significantly improved photo catalytic performances.

To conclude, the layered $Bi_2O(OH)_2SO_4$ compound has been developed as a new, wide band-gap photo catalyst. The co-presence of both hydroxyl and sulfate anion, as well as its unique layered structure mainly endow $Bi_2O(OH)_2SO_4$ with a high photo catalytic properties. The PDOS and TDOS results reveal that the intercalated SO_4^{2-} is mainly responsible for the wide band gap and highly positive VB. The study would provide an important strategy to develop new photo catalysts by grouping anions with the existing oxides or sulfides photo catalysts.

Methods

Sample preparation. All the reagents were analytical grade, purchased from Shanghai chemical company in China and used without further purification. $Bi_2O(OH)_2SO_4$ was synthesized by a simple water-bath method. Typically, 1 mmol $Bi(NO_3)_3{\cdot}5H_2O$ was added into 30 mL distilled water at room temperature under stirring, until the Bi(III) ions dissolve completely. Then, 1 mmol Na_2SO_4 was added to the system above. The mixture was heated at 60°C for 6 h in water bath. After reaction, the pH value of supernatant is determined to be about 1–2. The resultant precipitate was washed with distilled water and absolute ethanol for several times, respectively. Finally the sample was dried at 60°C for 6 h.

Sample characterizations. The crystal structures of the samples were determined by X-ray powder polycrystalline diffractometer (Rigaku D/max-2550VB), using graphite monochromatized Cu K_α radiation (λ = 0.154 nm), operating at 40 kV and 50 mA. The XRD patterns were obtained in the range of 20–80° (2θ) at a scanning rate of 7° min-1. The samples were characterized on a scanning electron microscope (SEM, Hitachi SU-1510) with an acceleration voltage of 15 keV. The samples were coated with 5-nm-thick gold layer before observations. The fine surface structures of the samples were determined by high-resolution transmission electron microscopy (HRTEM, JEOL JEM-2100F) equipped with an electron diffraction (ED) attachment with an acceleration voltage of 200 kV. UV-vis diffused reflectance spectra (UV-DRS) of the samples were obtained using a UV-vis spectrophotometer (UV-2550, Shimadzu, Japan). $BaSO_4$ was used as a reflectance standard in a UV-vis diffuse

reflectance experiment. Nitrogen sorption isotherms were performed at 77 K and $< 10^{-4}$ bar on a Micromeritics ASAP2010 gas adsorption analyzer. Each sample was degassed at 150°C for 5 h before measurements. Surface area was calculated by the Brunauer-Emmett-Teller (BET) method.

Measurements of photocurrents and EIS. An electrochemical system (CHI-660B, China) was employed to measure the photocurrents and electrochemical impedance spectroscopy (EIS). Electrochemical impedance spectroscopy (EIS) was performed from 0.1 Hz to 100 kHz at an open circuit potential of 0.3 V and an alternating current (AC) voltage amplitude of 5 mV. The data were analyzed by ZSimWin software. Photocurrent measurements were carried out in a conventional three-electrode system, in which indium-tin oxide (ITO) glass was used as the current collector to fabricate photo electrode, and 0.1 M Na_2SO_4 was used as the electrolyte solution. TiO_2/ITO and $Bi_2O(OH)_2SO_4$/ITO photo electrode were prepared by a dip-coating method. The photo electrode was implemented as the photo anode in a photoelectrochemical cell (PEC). IPCE measurement of $Bi_2O(OH)_2SO_4$ under air mass (AM) 1.5 illumination coupled with a series of band-pass filters.

Evaluation of photo catalytic activity. The photo catalytic activity of the sample was evaluated by the degradation of rhodamine B (RhB) aqueous solution under UV light ($\lambda < 420$ nm), using a 300 W Xe arc lamp (CEL-HXF 300) equipped with an ultraviolet cutoff filter as a light source. The photo reaction system was placed in a sealed black box with the top opened, and was maintained a distance of 15 cm from the light source. The photo catalysts (100 mg) were dispersed in 200 mL of 10 mg/L RhB aqueous solution in a Pyrex beaker at room temperature. Before lamp was turned on, the suspension was continuously stirred for 30 min in the dark to ensure the establishment of an adsorption–desorption equilibrium between the catalysts and RhB. During degradation, 3 mL of solution was collected at an interval of irradiation by pipette, and subsequently centrifuged to remove the photo catalysts. UV-vis spectra were recorded on a Spectrumlab 722sp spectrophotometer to determine the concentration of RhB. The photo catalytic activity is characterized by an apparent first-order rate constant (k_a), which can be calculated using Equation (4) as follows:

$$\ln(C_0/C) = k_a \times t, \text{ or } C = C_0 \times \exp(-k_a \times t) \quad (4)$$

Where C_0 is the initial concentration of RhB solution, and C is the concentration of RhB at t-min irradiation.

Theoretical calculations. The simulations of band structures, total and partial densities of states (DOS) were calculated by density functional theory (DFT) as implemented in the CASTEP. The calculations were carried out using the generalized gradient approximation (GGA) level, and Perdew-Burke-Ernzerh (PBE) formalism for combination of exchange and correlation function. The cut-off energy is chosen as 380 eV, and a density of ($3 \times 2 \times 5$) Monkhorst-Pack K-point was adopted to sample the Brillouin zone.

1. Fujishima, A. & Honda, K. Electrochemical photolysis of water at a semiconductor electrode. *Nature* **238**, 37–38 (1972).
2. Xu, X. X., Randorn, C., Efstathiou, P. & Irvine, J. S. T. A red metallic oxide photo catalyst. *Nat. Mater.* **11**, 595–598 (2012).
3. Iwase, A., Ng, Y. H., Ishiguro, Y., Kudo, A. & Amal, R. Reduced graphene oxide as a solid-state electron mediator in Z-scheme photo catalytic water splitting under visible light. *J. Am. Chem. Soc.* **133**, 11054–11057 (2011).
4. Linford, M. R., Auch, M. & Mohwald, H. Nonmonotonic effect of ionic strength on surface dye extraction during dye−polyelectrolyte multilayer formation. *J. Am. Chem. Soc.* **120**, 178–182 (1998).
5. Zhao, Y. X., Shi, H. X., Chen, M. D. & Teng, F. Splitting growth of novel CuO straw sheaves and their improved photo catalytic activity due to exposed active {110} facets and crystallinity. *CrystEngComm.* **16**, 2417–2423 (2014).
6. Xiao, F. X., Miao, J. W. & Liu, B. Layer-by-layer self-assembly of CdS quantum dots/graphene nanosheets hybrid films for photoelectrochemical and photo catalytic applications. *J. Am. Chem. Soc.* **136**, 1559–1569 (2014).
7. Lang, X. J., Chen, X. D. & Zhao, J. C. Heterogeneous visible light photo catalysis for selective organic transformations. *Chem. Soc. Rev.* **43**, 473–486 (2014).
8. Wang, X. C. *et al.* A metal-free polymeric photo catalyst for hydrogen production from water under visible light. *Nat. Mater.* **8**, 76–80 (2009).
9. Qi, D. P. *et al.* Bio-inspired antireflective hetero-nanojunctions with enhanced photoactivity. *Nanoscale* **5**, 12383–12387 (2013).
10. Zhang, Y. Y. *et al.* Three-dimensional CdS–titanate composite nanomaterials for enhanced visible-light-driven hydrogen evolution. *Small* **9**, 996–1002 (2013).
11. Tang, Y. X. *et al.* Efficient Ag@AgCl cubic cage photo catalysts profit from ultrafast plasmon-induced electron transfer processes. *Adv. Funct. Mater.* **23**, 2932–2940 (2013).
12. Yi, Z. G. *et al.* An orthophosphate semiconductor with photooxidation properties under visible-light irradiation. *Nat. Mater.* **9**, 559–564 (2010).
13. Pan, C. S. & Zhu, Y. F. New type of $BiPO_4$ oxy-acid salt photo catalyst with high photo catalytic activity on degradation of dye, *Environ. Sci. Technol.* **44**, 5570–5574 (2010).
14. Wang, J. *et al.* Facile synthesis of novel Ag_3PO_4 tetrapods and the {110} facets-dominated photo catalytic activity. *CrystEngComm.* **15**, 39–40 (2013).
15. Li, M., Chen, M. D., Wang, J. & Teng, F. Branching growth of novel silver phosphate dendrites and the greatly improved photo catalytic activity by the active {110} facets. *CrystEngComm.* **16**, 1237–1240 (2014).
16. Li, J., Zhang, L. Z., Li, Y. J. & Yu, Y. Synthesis and internal electric field dependent photoreactivity of Bi_3O_4Cl single-crystalline nanosheets with high {001} facet exposure percentages. *Nanoscale* **6**, 167–71 (2014).
17. Zheng, Y., Duan, F., Chen, M. Q. & Xie, Y. Synthetic $Bi_2O_2CO_3$ nanostructures: novel photo catalyst with controlled special surface exposed. *J. Mol. Catal. A.* **317**, 34–40 (2010).
18. Wang, G. *et al.* $Cu_2(OH)PO_4$: a near-infrared-activated photo catalyst. *Angew. Chem. Int. Ed.* **52**, 4810–4813 (2013).
19. Fu, X. L. *et al.* Hydroxide $ZnSn(OH)_6$: A promising new photo catalyst for benzene degradation. *Appl. Catal., B.* **91**, 67–72 (2009).
20. Yan, T. J. *et al.* Efficient photo catalytic degradation of volatile organic compounds by porous indium hydroxide nanocrystals. *Environ. Sci. Technol.* **44**, 1380–1385 (2010).
21. Sun, M. *et al.* Microwave hydrothermal synthesis of calcium antimony oxide hydroxide with high photo catalytic activity toward benzene. *Environ. Sci. Technol.* **43**, 7877–7882 (2009).
22. Mohapatra, P. & Parida, K. M. Photo catalytic activity of sulfate modified titania 3: Decolorization of methylene blue in aqueous solution. *J. Mol. Catal. A.* **258**, 118–123 (2006).
23. Huang, H. W., He, Y., Lin, Z. H., Kang, L. & Zhang, Y. H. Two novel Bi-based borate photo catalysts: crystal structure, electronic structure, photoelectrochemical properties, and photo catalytic activity under simulated solar light irradiation. *J. Phys. Chem. C.* **117**, 22986–22994 (2013).
24. Golic, L., Graunar, M. & Lazarini, F. Catena-Di-hydroxo-3-oxo-dibismuth(III) sulfate. *Acta. Cryst.* **B38**, 2881–2883 (1982).
25. Zhao, X., Qu, J. H., Liu, H. J. & Hu, C. Photoelectrocatalytic degradation of triazine-containing azo dyes at gamma-Bi_2MoO_6 film electrode under visible light irradiation (lamda > 420 nm). *Environ. Sci. Technol.* **41**, 6802–6807 (2007).
26. Zhang, C. & Zhu, Y. F. Synthesis of square Bi_2WO_6 nanoplates as high-activity visible-light-driven photo catalysts. *Chem. Mater.* **17**, 3537–3545 (2005).
27. Chen, R. G. *et al.* Template-free hydrothermal synthesis and photo catalytic performances of novel Bi_2SiO_5 nanosheets. *Inorg. Chem.* **48**, 9072–9076 (2009).
28. Cheng, H. F., Huang, B. B. & Dai, Y. Engineering BiOX (X = Cl, Br, I) nanostructures for highly efficient photo catalytic applications. *Nanoscale* **6**, 2009–2026 (2014).
29. Wu, C., Shen, L., Huang, Q. L. & Zhang, Y. C. Hydrothermal synthesis and characterization of Bi_2O_3 nanowires. *Mater. Lett.* **65**, 1134–1136 (2011).
30. Zhang, K. L., Liu, C. M., Huang, F. Q., Zheng, C. & Wang, W. D. Study of the electronic structure and photo catalytic activity of the BiOCl photo catalyst. *Appl. Catal., B.* **68**, 125–129 (2006).
31. Sun, S. M. *et al.* Visible light-induced efficient contaminant removal by Bi_5O_7I. *Environ. Sci. Technol.* **43**, 2005–2010 (2009).
32. Nethercot, A. H. Prediction of Fermi energies and photoelectric thresholds based on electronegativity concepts. *Phys. Rev. Lett.* **33**, 1088–1091 (1974).
33. Kudo, A., Kato, H. & Nakagawa, S. Water splitting into H_2 and O_2 on New $Sr_2M_2O_7$ (M = Nb and Ta) photo catalysts with layered perovskite structures: factors affecting the photo catalytic activity. *J. Phys. Chem. B.* **104**, 571–575 (2000).
34. Tang, J. W., Zou, Z. G. & Ye, J. H. Efficient photo catalytic decomposition of organic contaminants over $CaBi_2O_4$ under visible-light irradiation. *Angew. Chem. Int. Ed.* **43**, 4463–4466 (2004).
35. Wei, W., Dai, Y. & Huang, B. B. First principle characterization of Bi-based photo catalysts: $Bi_{12}TiO_{20}$, $Bi_2Ti_2O_7$ and $Bi_4Ti_3O_{12}$. *J. Phys. Chem. C.* **113**, 5658–5663 (2009).
36. Shi, R., Xu, T. G., Zhu, Y. F. & Zhou, J. High photo catalytic activity of oxychloride $CaBiO_2Cl$ under visible light irradiation. *CrystEngComm.* **14**, 6257–6263 (2012).
37. Zhang, L. S. *et al.* Sonochemical synthesisof nanocrystallite Bi_2O_3 as a visible-light-driven photo-catalyst. *Appl. Catal. A.* **308**, 105–110 (2006).
38. Walsh, A., Yan, Y. F., Huda, M. N., Al-Jassim, M. M. & Wei, S. H. Band edge electronic structure of $BiVO_4$: elucidating the role of the Bi s and V d orbitals. *Chem. Mater.* **21**, 547–551 (2009).
39. Kudo, A., Omori, K. & Kato, H. A novel aqueous process for preparation of crystal form-controlled and highly crystalline $BiVO_4$ powder from layered vanadates at room temperature and its photo catalytic and photophysical properties. *J. Am. Chem. Soc.* **121**, 11459–11467 (1999).
40. Bi, J. *et al.* Simple solvothermal routes to synthesize nanocrystalline Bi_2MoO_6 photo catalyst with different morphology. *Acta Mater.* **55**, 4699–4670 (2007).
41. Jiang, Y. Y., Zhang, J. W., Hu, Z. Q. & Liu, J. X. Synthesis and visible light photo catalytic activity of spinel MAl_2O_4 (M = Mg, Zn, Cu). *Appl. Mech. Mater.* **455**, 99–105 (2013).
42. Zhang, Y. H. *et al.* Identification of Bi_2WO_6 as a highly selective visible light photo catalyst toward oxidation of glycerol to dihydroxyacetone in water. *Chem. Sci.* **4**, 1820–1824 (2013).
43. Wang, K. *et al.* Highly efficient photodegradation of RhB–MO mixture dye wastewater byAg_3PO_4 dodecahedrons under acidic condition. *J. Mol. Catal. A.* **393**, 302–308 (2014).
44. Jiang, Z. L. *et al.* Understanding the role of nanostructures for efficient hydrogen generation on immobilized photo catalysts. *Adv. Energy Mater.* **3**, 1368–1380 (2013).

45. Wang, X. T. *et al*. Programmable photo-electrochemical hydrogen evolution based on multi-segmented CdS-Au nanorod arrays. *Adv. Mater.* **26**, 3506–3512 (2014).
46. Jiang, J., Zhao, K., Xiao, X. Y. & Zhang, L. Z. Synthesis and facet-dependent photoreactivity of BiOCl single-crystalline nanosheets. *J. Am. Chem. Soc.* **134**, 4473–4476 (2012).
47. Meng, S. G. *et al*. Sonochemical synthesis, characterization and photo catalytic properties of a novel cube-shaped $CaSn(OH)_6$. *Catal. Commun.* **12**, 972–975 (2011).
48. Cong, R. H. *et al*. Experimental and theoretical studies of second harmonic generation for $Bi_2O_2[NO_3(OH)]$. *Mater. Res. Bull.* **47**, 2573–2578 (2012).

Acknowledgments

This work is financially supported by National Science Foundation of China (21377060, 21103049), the Project Funded by the Science and Technology Infrastructure Program of Jiangsu (BM201380277, 2013139), Jiangsu Science Foundation of China (BK2012862), Six Talent Climax Foundation of Jiangsu (20100292), Jiangsu Province of Academic Scientific Research Industrialization Projects (JHB2012-10, JH10-17), the Key Project of Environmental Protection Program of Jiangsu (2013016, 2012028), A Project Funded by the Priority Academic Program Development of Jiangsu Higher Education Institutions (PAPD) and Jiangsu Province Innovation Platform for Superiority Subject of Environmental Science and Engineering sponsored by SRF for ROCS, SEM (2013S002) and "333" Outstanding Youth Scientist Foundation of Jiangsu (2011015). Besides, we are thankful to Miss K. Wu at Hunan University of Arts and Science for the language improvement.

Author contributions

H.T. performed the experiment and wrote the main text. F.T. designed the experiment, revised the paper and provided the financial support; J.X. performed UV-DRS characterization, prepared Figure 2 and wrote this part; S.L. performed the EIS test, prepared Figure 6 and wrote this part. N.L. prepared the Figure 5; Y.Z. performed the calculation and prepared the Figure 3; M.C. made the SEM and HRTEM characterization and revised the paper. All authors discussed the results and commented on the manuscript. All authors have reviewed the manuscript.

Additional information

Supplementary information accompanies this paper at http://www.nature.com/scientificreports

Competing financial interests: The authors declare no competing financial interests.

How to cite this article: Tian, H. *et al*. An Innovative Anion Regulation Strategy for Energy Bands of Semiconductors: A Case from Bi_2O_3 to $Bi_2O(OH)_2SO_4$. *Sci. Rep.* **5**, 7770; DOI:10.1038/srep07770 (2015).